Biophysical Journal
Article

Biophysical Society

Imaging Flow Cytometry Illuminates New Dimensions of Amyloid Peptide-Membrane Interactions

Reut Israeli,[1] Sofiya Kolusheva,[1,2] Uzi Hadad,[1,2] and Raz Jelinek[1,2,*]
[1]Department of Chemistry and [2]Ilse Katz Institute for Nanoscale Science and Technology, Ben-Gurion University of the Negev, Beersheba, Israel

ABSTRACT Membrane interactions of amyloidogenic proteins constitute central determinants both in protein aggregation as well as in amyloid cytotoxicity. Most reported studies of amyloid peptide-membrane interactions have employed model membrane systems combined with application of spectroscopy methods or microscopy analysis of individual binding events. Here, we applied for the first time, to our knowledge, imaging flow cytometry for investigating interactions of representative amyloidogenic peptides, namely, the 106–126 fragment of prion protein (PrP(106–126)) and the human islet amyloid polypeptide (hIAPP), with giant lipid vesicles. Imaging flow cytometry was also applied to examine the inhibition of PrP(106–126)-membrane interactions by epigallocatechin gallate, a known modulator of amyloid peptide aggregation. We show that imaging flow cytometry provided comprehensive population-based statistical information upon morphology changes of the vesicles induced by PrP(106–126) and hIAPP. Specifically, the experiments reveal that both PrP(106–126) and hIAPP induced dramatic transformations of the vesicles, specifically disruption of the spherical shapes, reduction of vesicle circularity, lobe formation, and modulation of vesicle compactness. Interesting differences, however, were apparent between the impact of the two peptides upon the model membranes. The morphology analysis also showed that epigallocatechin gallate ameliorated vesicle disruption by PrP(106–126). Overall, this study demonstrates that imaging flow cytometry provides powerful means for disclosing population-based morphological membrane transformations induced by amyloidogenic peptides and their inhibition by aggregation modulators.

SIGNIFICANCE Investigating membrane interactions of amyloid peptides is important for elucidating their physiological effects. Although microscopy studies of amyloid/membrane interactions generally examine relatively few binding events, comprehensive, population-based analyses have been rare. To our knowledge, this work demonstrates, for the first time, application of imaging flow cytometry for investigating interactions of representative amyloidogenic peptides with giant lipid vesicles. The experiments reveal dramatic population-based effects of the peptides upon distinct parameters pertaining to vesicle morphology and furthermore demonstrate significant differences between the effects of the two peptides. The experiments also show that a protein aggregation inhibitor effectively shields the vesicles from peptide-induced morphology changes. This study demonstrates that imaging flow cytometry provides a powerful platform for investigating morphological membrane transformations induced by amyloidogenic peptides.

INTRODUCTION

Prion proteins (PrPs) are associated with transmissible spongiform encephalopathies affecting both animals and humans, which are also known as the "prion diseases" (1,2). Whereas cellular PrP (PrP^C) is a soluble protein found in the central nervous system, its conformational isomer scrapie PrP ($PrPS^C$) undergoes fibrillation and is considered to be the infectious agent (1,2). The mechanisms by which $PrPS^C$ aggregates induce neurotoxicity are still elusive; however, it is believed that interactions between prions and lipid membrane aid conversion of PrP^C to $PrPS^C$ (3–7) and contribute to cytotoxicity of the protein. PrP^C binds to negatively charged lipid membranes by electrostatic and hydrophobic interactions, which results in its partial insertion into the lipid bilayer (8). Membrane binding, conformational transformations, and aggregation states of PrP are intimately affected by membrane compositions

Submitted July 23, 2019, and accepted for publication January 15, 2020.
*Correspondence: razj@bgu.ac.il
Editor: Tommy Nylander.
https://doi.org/10.1016/j.bpj.2020.01.018

(e.g., the presence of putative glycosylphosphatidylinositol anchors (5,6)) and other parameters such as solution pH (7). However, the precise relationship between membrane interactions of PrP and its biological activity has not been fully elucidated yet.

The 106–126 fragment of PrP (PrP(106–126)), derived from the full-length PrP, is believed to constitute the principal amyloidogenic determinant of the protein. PrP(106–126) has been observed in almost all PrP isoforms extracted from brains of patients suffering from prion diseases (8). This peptide forms both amyloid fibrils and cytotoxic oligomers, which resemble those assembled by the full-length protein (9,10). PrP(106–126) has been shown to interact with and disrupt membrane models with different compositions (11); the peptide has also been shown to modulate membrane viscosity (9) and form pores in planar lipid bilayers (12,13).

A potential therapeutic strategy for combating protein misfolding diseases has been based upon identification of (usually small) molecules that inhibit or otherwise interfere with aggregation of amyloidogenic proteins (14,15). Previous studies have shown that the polyphenols, especially (−)-epigallocatechin gallate (EGCG), extracted from green tea, modulate misfolding pathways of amyloid proteins, including prions (16,17). EGCG is believed to directly bind to unfolded polypeptide chains, inhibiting β-sheet formation, which is an early event in amyloid assembly (18).

Islet amyloid polypeptide (IAPP), also called amylin, is a 37-residue peptide secreted in conjunction with insulin; it is highly amyloidogenic and often found in amyloid deposits in patients with type II diabetes (19,20). IAPP aggregates have been found in 90% of patients with diabetes, and the peptide has been intensely studied for possible role in the loss of β-cell mass (21). The molecular mechanism of IAPP cytotoxicity has not been determined; however, membrane interactions of the peptide are believed to constitute major toxic determinants (22,23). In particular, human IAPP (hIAPP) oligomeric species have been implicated in membrane interactions and cytotoxicity (24,25). Molecular dynamics simulations revealed that hIAPP monomers bind lipid bilayers in distinct orientations (26). Previous studies have linked membrane disruption by hIAPP to induction of pronounced bilayer curvature (27), pore formation (28), detergent effects (29), and other putative mechanisms.

Lipid vesicles have been the primary "workhorse" for analysis of membrane interactions of amyloid proteins (and membrane-active peptides in general). Most studies have utilized spectroscopic methods, employing small or large vesicles, to analyze peptide-membrane interactions (30–33). Although such experiments can provide a wealth of structural and functional information on peptides and the membrane and their interactions, microscopic evaluation of amyloid-protein morphological impact on membranes has been particularly sought because these scenarios mimic the "real life" situation of peptides affecting membranes of actual cells in the body. In this context, giant vesicles (GVs) have been employed for microscopic investigations of amyloid-protein/membrane interactions (34,35). Although conventional optical microscopy and particularly fluorescence microscopy are useful for visualizing protein/GV interactions, it should be noted that analysis of individual microscopy images of GVs (and the impact of peptides on the vesicles) is generally subjective and prone to wide variability. Statistical microscopic evaluation of larger populations of GVs is feasible in principle; however, this approach is cumbersome and time consuming.

Imaging flow cytometry is a powerful bioanalytical technique, providing comprehensive structural information on populations of micrometer-scale particles. This technique combines the population screening capabilities of flow cytometry, with morphological analysis of particles by microscopic imaging. Imaging flow cytometry has been previously used in cell studies, providing statistical information on morphology changes occurring in response to biological and chemical stimuli (36). In essence, imaging flow cytometry offers multiparametric morphological information on diverse cellular events (37). The technique has been employed, for example, for assessment of apoptosis-induced changes in nuclear morphology (38), intercellular communication by exchange of cytoplasmic material (39) as an in vivo imaging platform for tracking immunotherapeutic cells (40), and for studying cellular uptake of nanoparticles (41).

Here, we present application of imaging flow cytometry for studying morphological transformations of GVs induced by PrP(106–126), hIAPP, and the effect of EGCG, an aggregation modulator, upon membrane interactions of the prion peptide. Notably, to the best of our knowledge, imaging flow cytometry has not been previously used for analysis of GV interactions of amyloidogenic proteins. The experiments reveal that PrP(106–126) and hIAPP intimately altered the shape, surface features, and compactness of fluorescently labeled GVs. Importantly, preincubation of PrP(106–126) with EGCG before incubation with the vesicles resulted in attenuation of membrane disruption, attesting to the "membrane shielding" effect of EGCG. This work demonstrates that imaging flow cytometry offers new, to our knowledge, analytical capabilities for better understanding membrane interactions of amyloidogenic peptides.

MATERIALS AND METHODS

Materials

PrP(106–126) having the amino acid sequence KTNMKHMAGAAAA GAVVGGLG (single-letter code) was purchased from Peptron (Daejeon, South Korea) in a lyophilized form at 95% purity. HIAPP (amylin, human) was purchased from AnaSpec (Fremont, CA). A fluorescently labeled PrP(106–126) peptide, that is, H-cys(solfu-cy5)-KTNMKHMAGAAAAG AVVGGLG-NH_2, was purchased from JPT Peptide Technologies (Berlin, Germany). (1,2-dioleoyl-sn-glycero-3-phospho-(1′-rac-glycerol) (DOPG),

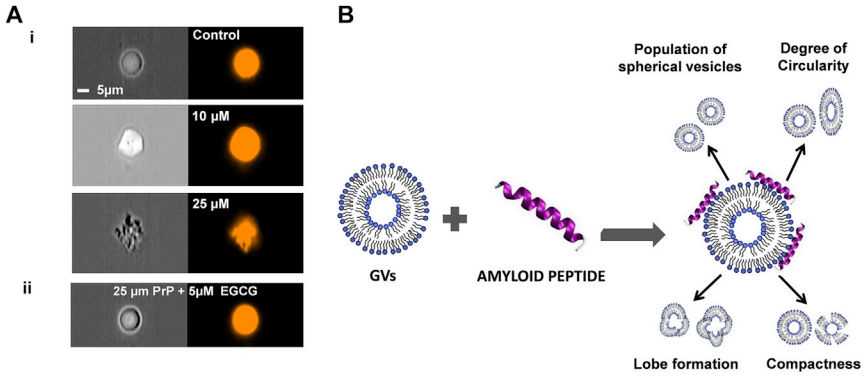

FIGURE 1 Principles of imaging flow cytometry applied to analyze interactions of PrP(106–126) with giant vesicles (GVs). (*A*) Representative bright-field (*left column*) and fluorescence images (excitation 488 nm, *right column*) of GVs incubated with different concentrations of PrP(106–126) and with EGCG are shown. The images were recorded by the imaging flow cytometer by applying a functional Erode mask. (*B*) Scheme depicting the morphological transformations of the GVs induced by amyloid peptides, as probed by imaging flow cytometry, is shown. To see this figure in color, go online.

(1,2-dioleoyl-sn-glycero-3-phosphocholine) (DOPC), and 1,2-dipalmitoyl-sn-glycero-3-phosphoethanolamine-N-(7-nitro-2-1,3-benzoxadiazol-4-yl) (NBD-PE) were purchased from Avanti Polar Lipids (Alabaster, AL). (−)-cis-3,3′,4′,5,5′,7-hexahydroxy-flavane-3-gallate, EGCG, 2-amino-2-(hydroxymethyl) propane-1,3-diol (Trizma base), and 1,1,1,3,3,3-hexafluoro-2-propanol (HFIP) were purchased from Sigma-Aldrich (St. Louis, MO).

Sample preparation

PrP(106–126) was dissolved in HFIP at a concentration of 2.5 mM, and hIAPP was dissolved in HFIP at a concentration of 0.5 mg/mL. Peptide samples were stored at −20°C until use to prevent aggregation. For each experiment, the solution was thawed, and the required amount was dried by evaporation for 6–7 h to remove the HFIP. The dried peptide samples were dissolved in 10 mM sodium phosphate (pH 7.4) at room temperature. Stock solutions of EGCG 200 μM in double-distilled H_2O were prepared and diluted into the PrP(106–126) solutions at the required concentrations. Peptide samples were incubated with the GVs for 10 min before measurements.

Preparation of GVs

GVs were prepared through a rapid evaporation method (42). Briefly, GVs comprising 0.25:0.75 DOPC/DOPG molar ratio dissolved in 1 mL chloroform in a 250 mL round-bottom flask. A quantity of 5 mL Tris buffer (10 mM (pH 7.4)) was added carefully with a pipette. The organic solvent was immediately removed by rotary evaporation under reduced pressure (final pressure 20 mbar) at room temperature. After evaporation of 4–5 min, the resulting vesicle solution exhibited a turbid appearance and was used on the day of preparation. Before drying, the vesicles were additionally supplemented with NBD-PE at a 500:1 mol ratio (total phospholipids: NBD-PE).

Imaging flow cytometry

The GVs were analyzed by Amnis ImageStreamX MK II imaging flow cytometer (Seattle, WA), acquiring 1000 images of GVs on average in the bright-field channel and the fluorescence emission channels using an excitation laser operating at 488 nm with 10 mW power (emission detection in 595–640 nm; objective 60× NA 0.75). Image analysis was carried out using Amnis IDEAS software. The initial identification of in-focus images of GVs was carried out using the system default mask of bright-field and gradient root mean square scores. The software uses algorithms based on pixel intensity and variation in an object image frame; essentially, the algorithm employs pixel intensity to spatially distinguish vesicle area from the surrounding background (43). For the purpose of calculating the shape feature values of GVs (aspect ratio intensity, circularity, compactness, and lobe count), Amnis Erode custom masks (e.g., a set of pixels enclosing the region of interest while discarding "edge" pixels) were applied to the fluorescence channel; such masks are created by the user through the Mask Manager interface using existing function masks in the analysis software. For aspect ratio calculations, the bright-field channel was employed using the default mask.

Circularity and compactness analysis

The circularity values were extracted by the Amins software by measuring the radii of the GVs (considered as centroids) in different regions within the particles. Essentially, the circularity constitutes a calculated index, which is inversely related to the variance of these radii. The compactness value measures the degree of how well the object is packed together. This feature includes all the intensity-weighted pixels within the mask. The higher the value, the more condensed the object.

RESULTS

The aim of this study is to employ imaging flow cytometry as a new, to our knowledge, strategy for studying membrane interactions of PrP(106–126) and hIAPP, respectively, and for assessing the impact of aggregation modulators such as EGCG upon membrane interactions of the prion peptide. Fig. 1 illustrates the experimental strategy and information garnered. Fig. 1 *A* depicts representative fluorescence microscopy images recorded in the imaging flow cytometer after incubation of PrP(106–126) with fluorescently labeled GVs comprising NBD-PE/DOPC/DOPG 0.004:0.25:0.75 mol ratio).

Although microscopy analysis of individual vesicles, such as presented in Fig. 1 *A*, can yield valuable information upon amyloid/membrane interactions, the (rather subjective) visual evaluation of single vesicles limits the potential contributions and significance of such microscopy experiments for providing in-depth understanding of peptide-membrane interactions. Indeed, even analysis of multiple vesicles by microscopy inspection poses significant technical and interpretational hurdles because of the variability in vesicle sizes and shapes (see, for example, cryogenic transmission electron microscopy images in Fig. S1). In comparison, population-based statistical image analysis, schematically outlined in Fig. 1 *B* and presented in Figs. 2, 3, 4, and 5, which is the core of the imaging flow cytometry approach, can provide comprehensive information upon

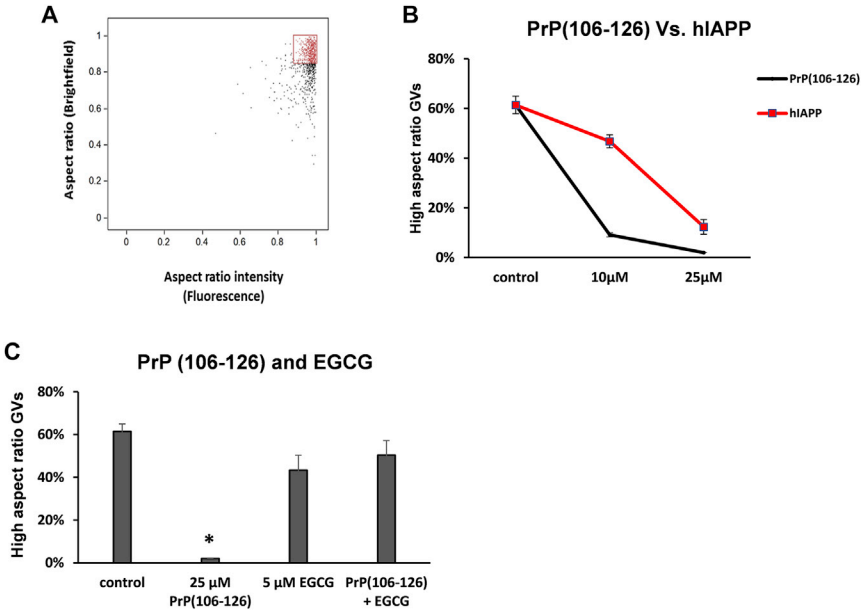

FIGURE 2 Effect of amyloid peptide addition upon the percentage of spherical vesicles. (*A*) Imaging flow cytometry analysis illustrates the aspect ratios (recorded in both the bright-field (*y* axis) and fluorescence (*x* axis) fields) of GVs (1 mM). The red square at the top right accounts for the population of the most spherical vesicles (aspect ratios close to 1.0). (*B*) Populations of spherical GVs (corresponding to the *red square* in the data set shown in (*A*) induced by PrP(106–126) or hIAPP are shown. (*C*) Changes in the percentage of spherical GVs induced by both PrP(106–126) and EGCG ($*p < 0.05$) are shown. To see this figure in color, go online.

the impact of amyloid peptides such as PrP(106–126) and hIAPP upon vesicle morphologies, sizes, and densities, and illuminate the inhibitory effect of aggregation modulators such as EGCG.

Fig. 1 *B* schematically illustrates the statistical structural information gleaned from imaging flow cytometry analysis. Specifically, the technique provides detailed statistical information upon morphological transformations of the vesicles, including the percentage of spherical vesicles in the overall vesicle population, degree of vesicle circularity, formation of lobes, and vesicle compactness (Fig. 1 *B*). Importantly, the experimental data in Figs. 2, 3, 4, and 5 demonstrate that PrP(106–126) and hIAPP both intimately modulated all these parameters, providing a powerful means for investigating bilayer interactions of the peptides and the effect of aggregation modulators such as EGCG upon peptide-membrane interactions.

Fig. 2 presents imaging flow cytometry analysis of the effects of PrP(106–126) and hIAPP upon the percentage of fluorescent spherical vesicles in the NBD-PE/DOPG/DOPC GV population. Notably, numerous studies have determined that both peptides experience pronounced affinity to membrane bilayers; partition coefficient analysis we carried out indicates that the two peptides exhibit significant and similar vesicle binding (Table S1). The graph in Fig. 2 *A* illustrates a flow cytometry data set recorded after the addition of PrP(106–126) to the GV sample, in which each dot corresponds to a vesicle imaged and analyzed by the instrument according to the desired parameter, namely, the vesical aspect ratio in our case. Specifically, Fig. 2 *A* shows the distribution of GVs according to the bright-field aspect ratio (the *y* axis) and fluorescence aspect ratio (*x* axis) in the control sample (before addition of PrP(106–126)). The red square at the top right in Fig. 2 *A* accounts for the population

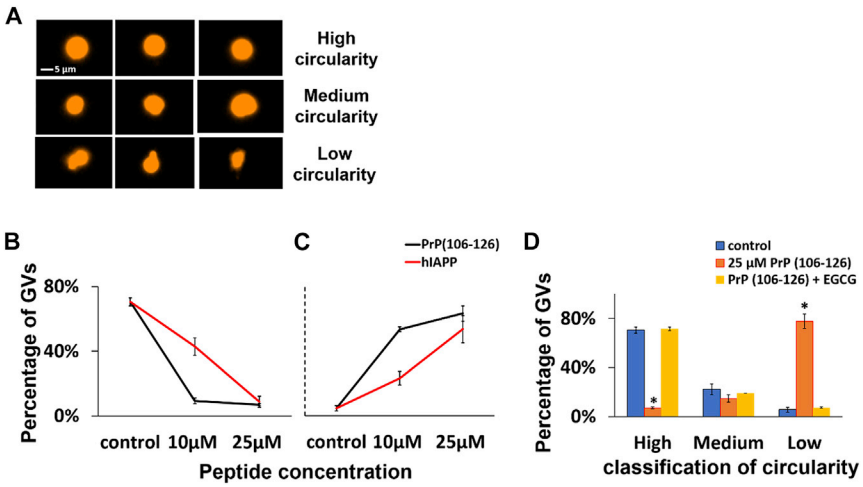

FIGURE 3 Statistical analysis of vesicle circularity. (*A*) Representative images of GVs with different circularity classifications are shown. (*B*) Populations of high-circularity GVs after addition of PrP(106–126) or hIAPP are shown. (*C*) Populations of low-circularity GVs after addition of PrP(106–126) or hIAPP are shown. (*D*) GVs incubated with EGCG (5 μM) and PrP(106–126) (25 μM) are shown. Analysis was conducted on ~500 objects; $*p < 0.05$. To see this figure in color, go online.

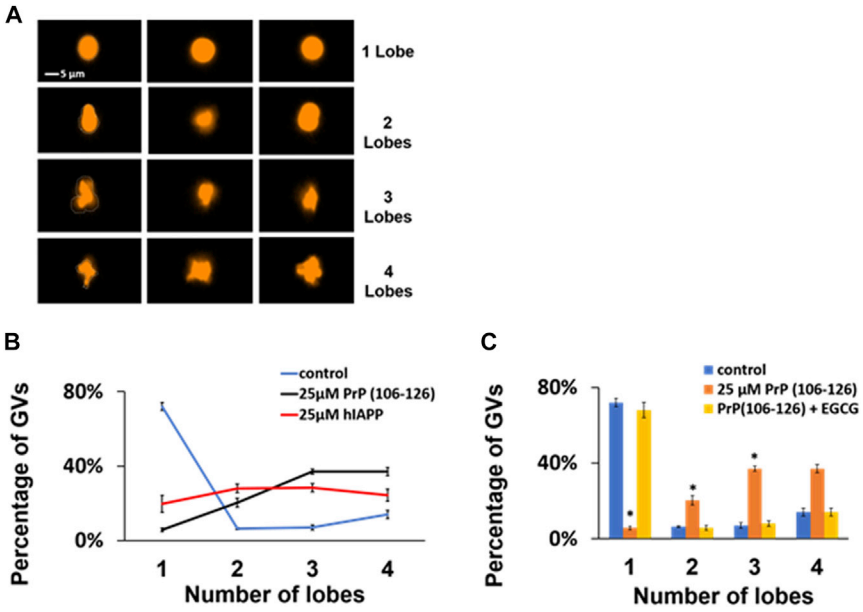

FIGURE 4 Lobe count analysis. (*A*) Representative images of GVs exhibiting different lobe counts are shown. Lobe count was based upon the selected population of fluorescent GV images. (*B*) GV subpopulations distributed according to the number of lobes after addition of different concentrations of PrP(106–126) and hIAPP are shown. (*C*) GV subpopulations after incubation of EGCG (5 μM) with PrP(106–126) (25 μM) are shown. Analysis was conducted on ~500 objects; $*p < 0.05$. To see this figure in color, go online.

of vesicles exhibiting aspect ratios closer to unity, both in the bright-field and fluorescence analyses, that is, the population of the most spherical vesicles.

Fig. 2 *B* compares the effect of PrP(106–126) and hIAPP upon the percentage of spherical vesicles in the GV populations. The graph in Fig. 2 *B* reveals that as the concentration of PrP(106–126) increases, the percentage of spherical GVs (e.g., vesicles recorded in the red square in Fig. 2 *A*) was significantly reduced, reaching around 10% when 10 μM PrP(106–126) was added to the vesicle solution and ~2% in the sample containing 25 μM peptide concentration. The lesser abundance of spherical vesicles upon addition of PrP(106–126) in Fig. 2 *B* is ascribed to interactions of the peptide with the lipid bilayer, resulting in vesicle distortion and reduction of spherical shape. Indeed, the elimination of spherical vesicle population apparent in Fig. 2 *B* echoes the microscopy images of the single vesicles in Fig. 1 *A*.

In contrast to PrP(106–126), Fig. 2 *B* indicates that hIAPP induced significantly lower disruption of the spherical GVs. Specifically, addition of 10 μM hIAPP reduced the percentage of spherical vesicles to 45%, whereas 25 μM addition resulted in ~18% population of spherical GVs. The lesser impact of hIAPP upon the vesicles is likely due to less pronounced bilayer interactions; indeed, less significant membrane interactions of hIAPP have been reported in concentrations below ~20 μM (44). The difference between the effects of PrP(106–126) and hIAPP upon the population of spherical vesicles, depicted in Fig. 2 *B*, exemplifies the power of imaging flow cytometry to furnish statistical information pertaining to distinct membrane interaction modes of the two amyloid peptides. Importantly, imaging flow

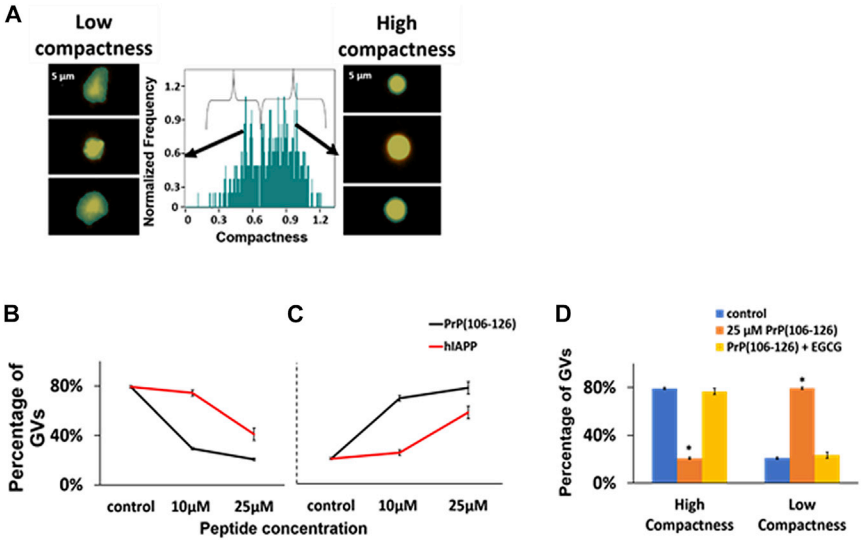

FIGURE 5 Vesicle compactness population analysis. (*A*) Representative images of GVs exhibiting different compactness values are shown. (*B* and *C*) GV subpopulations (high and low compactness in accordance) according to the relative compactness values after addition of different concentrations of PrP(106–126) and hIAPP are shown. (*D*) GVs incubated with PrP(106–126) (25 μM) and EGCG (5 μM) are shown. Analysis was conducted on ~500 objects; $*p < 0.05$. To see this figure in color, go online.

cytometry analysis of GV interactions with bovine serum albumin, a nonmembrane active protein employed as a control protein, showed no morphological transformations (Fig. S2).

A striking "vesicle protective" effect was apparent when EGCG was added concurrently with PrP(106–126) as shown in Fig. 2 *C*. Importantly, coaddition of PrP(106–126) (25 μM) and EGCG (5 μM) resulted in a very small change to the population of spherical vesicles (to 50%; Fig. 2 *C*). Specifically, addition of 5 μM EGCG alone induced a small decrease in the population of spherical vesicles (from around 65 to ~45%; Fig. S4), ascribed to the hydrophobic nature of this polyphenol (45). This result is consistent with the fluorescence microscopy results in Fig. 1 *A* and demonstrates that EGCG aid retention of spherical vesicles' population. The membrane shielding effect of EGCG, apparent in Fig. 2 *C*, is likely ascribed to inhibition of the assembly of membrane-active PrP(106–126) oligomers (45,46). The protective effect of EGCG on the membrane was more notable when EGCG was preincubated with PrP(106–126); however, the protection effect was retained also when EGCG was added to the GVs together, or after, addition of the peptide (Fig. S3).

Whereas Fig. 2 illuminates the modulation of spherical vesicle population after addition of PrP(106–126), Fig. 3 examines the effect of PrP(106–126) upon overall vesicle circularity in the high aspect ratio GV population (e.g., population within the *red square* in Fig. 2 *A*). The degree of circularity was determined through assessing vesicle shapes in the fluorescence channel deviating from a full circle. Fig. 3 *A* shows representative images of vesicles exhibiting different circularity classifications. Essentially, the circularity values are based upon utilizing "masks" (set of pixels recorded by the instrument from the region of interest). The circularity score is a measure of how much the cell radius varies (thus, highly spherical GVs possess high circularity scores, whereas irregularly shaped GVs have low circularity scores). The high circularity classification depicted in Fig. 3 *A* corresponds to calculated circularity scores between 20 and 30, medium is assigned to circularity scores between 10 and 20, and low circularity reflects GVs exhibiting scores under 10.

The impact of PrP(106–126) and hIAPP upon the population distributions of GVs among the high circularity and low circulation classifications is depicted in Fig. 3, *B* and *C*, respectively. Echoing Fig. 2 *B*, the graphs in Fig. 3, *B* and *C* indicate that both peptides induced substantial morphology changes. Specifically, addition of PrP(106–126) to the GV solution gave rise to a pronounced decrease in the percentage of high-circularity vesicles (Fig. 3 *B*), in parallel with an increase in the abundance of low-circularity GVs (Fig. 3 *C*). The observation of PrP(106–126)-induced distortion of vesicle shapes, reflected in the lower circularity outlined in Fig. 3, *B* and *C*, complements the aspect ratio analysis in Fig. 2 *B*, similarly reflecting the pronounced bilayer interactions of PrP(106–126).

Similar to the spherical population analysis in Fig. 2 *B*, the circularity results in Fig. 3, *B* and *C* demonstrate that hIAPP gave rise to more moderate transformations of GV shapes, reducing the percentage of high-circularity vesicles (Fig. 3 *B*) and increasing the percentage of low-circularity vesicles (Fig. 3 *C*) to a lesser extent than PrP(106–126). These results likely account for the lower degree of membrane disruption by hIAPP compared to PrP(106–126) in the peptide concentrations examined (46,47). We also applied circularity analysis for evaluation of the effect of EGCG upon PrP(106–126)-vesicle interactions (Fig. 3 *C*). EGCG alone (at a concentration of 5 μM) hardly affected the distribution of vesicles among the distinct circularity classifications (Fig. S3). Notably, when EGCG (5 μM) and PrP (106–126) (25 μM) were added together to the NBD-PE/DOPG/DOPC vesicles, the distribution of vesicle populations between high, medium, and low circularities resembled the control vesicles (before addition of either PrP (106–126) or EGCG), underscoring the bilayer-shielding effects of EGCG.

Although Figs. 2 and 3 report on the effect of PrP(106–126) upon vesicle circularity, we further assessed how the peptide modified finer details of vesicle shape and surface morphology through lobe count analysis (Fig. 4). Fig. 4 *A* illustrates representative images of vesicles and the assigned "lobe counts." The number of lobes of each vesicle was determined according to the distortion of the vesicles; an Erode mask was placed upon the vesicle, and the number of protrusions, namely, distortions from circular symmetry, determined the number of lobes, yielding values of one (circular shape), two (two lobes), etc. (Fig. 4 *A*).

The graph shown in Fig. 4 *B* illuminates the effects of peptide addition upon the lobe counts within the GV population. The correlation between peptide concentration and shape deformation of the vesicles, apparent in Fig. 4 *B*, is ascribed to bilayer perturbation by the peptide and corroborates the results in Figs. 2 and 3 pointing to a decrease in spherical vesicle population after peptide addition. Fig. 4 *B* shows that both PrP(106–126) and hIAPP significantly increased lobe counts as compared to the control vesicles (vesicle population before addition of the peptides). The increase in lobe count is consistent with the circularity data in Figs. 2 and 3, reflecting vesicle distortion after interaction with the peptides. Specifically, addition of 25 μM PrP(106–126) or 25 μM hIAPP resulted in dramatic reduction of one-lobe GVs in comparison to the control vesicle sample while significantly increasing the percentage of the two-lobe and three-lobe vesicles (Fig. 4 *B*). Consistent with the circularity analyses in Figs. 2 and 3, the lobe count data in Fig. 4 *B* indicate that PrP(106–126) induced more pronounced vesicle distortion in comparison to hIAPP, reflected in the lower percentage of one-lobe GVs (~5% after addition of PrP(106–126), ~20% for hIAPP) and higher percentage of the distorted three-lobe and four-lobe vesicles (~40% in case of PrP(106–126) compared to ~30% after addition of hIAPP).

Fig. 4 *C* displays the effect of EGCG upon the GV lobe count population analysis. EGCG by itself appears to induce vesicle deformation (i.e., higher abundance of vesicles exhibiting more than a single lobe), likely accounting for the hydrophobic nature of the molecule (Fig. S4). However, similar to the statistical results outlined in Figs. 2 and 3 above, when EGCG was added together with 25 μM PrP(106–126), it clearly inhibited vesicle distortion, giving rise to GVs exhibiting lower lobe counts compared to the addition of PrP(106–126) alone (e.g., Fig. 4 *B*). The quantitative statistical lobe count analysis in Fig. 4, *B* and *C* reveals both the significant vesicle shape deformation induced by PrP(106–126) (Fig. 4 *B*) and the protective effect of EGCG (Fig. 4 *C*).

Although the experimental data presented in Figs. 2, 3, and 4 account for the impact of PrP(106–126) and hIAPP upon the shape and structure of the NBD-PE/DOPC/DOPG GVs, imaging flow cytometry can also provide useful statistical information upon the effect of the peptides upon vesicle compactness (Fig. 5). The compactness is quantified through addition of the intensity-weighted fluorescent pixels within the imager masks placed upon each vesicle. Thus, higher values reflect more condensed vesicles, and, conversely, lower compactness accounts for more "spread out" vesicles. Fig. 5 *A* shows the histogram depicting the compactness distribution of GVs in a sample. In a fully spherical, unperturbed vesicle (Fig. 5 *A*, *right*), the fluorescence is distributed fairly evenly within the enclosed circular mask, and the calculated compactness is high. On the other hand, after addition of a membrane-active peptide such as PrP(106–126), the vesicle shape was significantly distorted and the resultant compactness was clearly lower as the vesicles lost their condensed spherical morphology (Fig. 5 *A*, *left*). As indicated in Fig. 5 *A*, we selected a compactness value of 0.75 as the divider value between "high-compactness" and "low-compactness" vesicles.

The statistical analyses in Fig. 5, *B* and *C* reveal that addition of PrP(106–126), and to lower extent hIAPP, reduced the vesicle compactness, that is, resulting in a higher population of low-compactness GVs and lower percentage of high-compactness GVs. These results are ascribed to disruption of the lipid bilayer by PrP(106–126) or hIAPP oligomers, resulting in partial vesicle disintegration (2,3). Similar to the results outlined in Figs. 2, 3, and 4, the compactness analyses in Fig. 5, *B* and *C* indicate more pronounced impact of PrP(106–126) compared to hIAPP, accounting for greater bilayer disruption of the former (46–49).

The compactness analysis in Fig. 5 *D* attests to the inhibitory effect of EGCG. Specifically, the bar diagram in Fig. 5 *C* depicts the distribution of low- and high-compactness vesicles upon coaddition of EGCG (5 μM) and PrP(106–126) (25 μM). Echoing the data presented in Figs. 2, 3, and 4, the diagram in Fig. 5 *C* demonstrates that EGCG effectively shielded the GVs, inhibiting vesicle interactions with PrP(106–126), thereby maintaining GV compactness close to the control sample (before addition of PrP(106–126)).

DISCUSSION

Deciphering the effects of PrP(106–126) and hIAPP upon the cellular membrane is important because membrane interactions may play fundamental roles in aggregation of both peptides and their cytotoxicity. Spectroscopic and diffraction methods have been useful in providing molecular information upon the impact of amyloid peptides such as PrP(106–126) and hIAPP on membrane bilayers. Imaging flow cytometry, in comparison, integrates microscopic evaluation of structural aspects events with a statistical, population-based analysis. In the experiments presented here, imaging flow cytometry enabled evaluation of structural transformations induced in GVs comprising fluorescently labeled DOPG/DOPC vesicles by PrP(106–126) or hIAPP. Furthermore, the experiments reveal the significant inhibitory effect of EGCG upon vesicle interactions of PrP(106–126).

The data presented here indicate that imaging flow cytometry is a powerful technique for elucidating the consequences of PrP(106–126)/hIAPP interactions with the GVs via statistical, population-based analysis. Importantly, in the concentrations examined, both PrP(106–126) and hIAPP had significant effects upon vesicle shape and surface features, in contrast to the effects of induced vesicle disintegration. These effects were exemplified in the reduction of overall vesicle circularity (Figs. 2 and 3), formation of "lobes" (Fig. 4), and lower vesicle compactness (Fig. 5). Although it has been proposed that both amyloid peptides affect pore formation in membrane bilayers (27,44–51), the information provided here points to significant cooperative/long-range effects upon the membrane. Although these membrane transformations might occur in parallel or in addition to pore formation, the imaging flow cytometry experiments appear to suggest that neither PrP(106–126) nor hIAPP induce complete membrane disintegration (often referred to as "detergent effect" or "micellization") (49). It should be noted, however, that the loss of vesicle compactness upon addition of PrP (106–126) or hIAPP (Fig. 5) might be accounted for by lipid release and/or pore formation.

In a broader context, it has been long hypothesized that membrane disruption by PrP(106–126) and hIAPP plays important roles in the pathological facets of the diseases associated with these peptides. Accordingly, employing imaging flow cytometry to probe significant population-based statistical bilayer transformations (such as compactness and circularity) provides invaluable evidence for the distinct effects of these amyloidogenic peptides upon membrane bilayers.

Notably, the imaging flow cytometry experiments reveal that differences exist between the effects of PrP(106–126)

and hIAPP (in the same concentrations) upon vesicle morphology. Indeed, the data demonstrate significantly greater impact of PrP(106–126) upon vesicle circularity (Fig. 3), lobe formation (Fig. 4), and compactness (Fig. 5). These differences may reflect more pronounced membrane interactions and bilayer reorganization induced by PrP(106–126). Although previous studies have shown distinct modes of membrane interactions by PrP(106–126) and hIAPP, a direct comparison between the effects of the two amyloid peptides upon vesicle structures, examined by imaging flow cytometry, has not been reported yet.

The imaging flow cytometry experiments also nicely illuminated the membrane shielding effect of EGCG, a widely studied protein aggregation inhibitor. Aggregation modulators such as EGCG have been shown to also interfere with membrane interactions of amyloid proteins, particularly through reducing populations of membrane-active oligomeric and prefibrillar species (18,52,53). The imaging flow cytometry results demonstrate quantitively that when added together with PrP (106–126), EGCG effectively shielded the lipid bilayer, significantly reducing the morphological transformations induced by the peptide.

This study highlights notable features of imaging flow cytometry for studying membrane interactions of amyloid peptides (and membrane-active peptides in general). In particular, the data illuminate distinct advantages of imaging flow cytometry in comparison to other microscopy techniques. Although confocal fluorescence microscopy and electron microscopy enable visualization of individual GVs and the effect of peptides upon their morphologies, these techniques are limited by practical aspects, including vesicle motion, broad distributions of vesicles' sizes and shapes, resolution of vesicle features, and long acquisition times. Imaging flow cytometry, on the other hand, is inherently a population-based technique, providing statistical information according to defined morphological parameters. The microscopy images are recorded automatically in the flow experiment without special preparation. As such, the technique facilitates acquisition and analysis of thousands of vesicle images in a short time, providing comprehensive statistical structural information upon large vesicle populations.

CONCLUSIONS

This study explores application of imaging flow cytometry for studying interactions of PrP(106–126), the amyloidogenic determinant of the PrP, and hIAPP, a short aggregating peptide associated with the pathologies of type II diabetes, with GVs. The experiments also explore the inhibition of PrP(106–126)/vesicle interactions by EGCG, an aggregation modulator. We show that imaging flow cytometry, which has not previously been applied for studying peptide-membrane interactions, provides comprehensive insight into membrane morphological modifications induced in fluorescently labeled NBD-PE/DOPG/DOPC GVs by PrP(106–126) or hIAPP. In particular, the experiments reveal population-wide factors pertaining to vesicle spherical features, surface protrusions (e.g., lobes), and vesicle compactness. The results both allow quantifying macroscale impact of PrP(106–126) or hIAPP upon membrane bilayers, demonstrating that the two peptides exhibit significantly different structural effects upon vesicle interactions, and demonstrate the inhibitory action of EGCG, which effectively "shielded" the vesicles from PrP(106–126)-induced morphological distortions. This work demonstrates that imaging flow cytometry may be employed as a powerful vehicle for studying interactions of amyloid peptides with membrane vesicles and membrane interactions of biomolecular species in general.

SUPPORTING MATERIAL

Supporting Material can be found online at https://doi.org/10.1016/j.bpj.2020.01.018.

AUTHOR CONTRIBUTIONS

R.I. and R.J. designed the experiments. R.I. and U.H. performed experiments and analyzed the data. R.I. and R.J. wrote the manuscript.

REFERENCES

1. Carleton, G. D., C. J. Gibbs, Jr., and M. Alpers. 1967. Transmission and passage of experimental "Kuru" to chimpanzees. *Science.* 155:212–214.
2. Simoneau, S., H. Rezaei, …, C. I. Lasmézas. 2007. In vitro and in vivo neurotoxicity of prion protein oligomers. *PLoS Pathog.* 3:e125.
3. Kazlauskaite, J., N. Sanghera, …, T. J. T. Pinheiro. 2003. Structural changes of the prion protein in lipid membranes leading to aggregation and fibrillization. *Biochemistry.* 42:3295–3304.
4. Sanghera, N., and T. J. Pinheiro. 2002. Binding of prion protein to lipid membranes and implications for prion conversion. *J. Mol. Biol.* 315:1241–1256.
5. Baron, G. S., A. G. Hughson, …, B. Caughey. 2011. Effect of glycans and the glycophosphatidylinositol anchor on strain dependent conformations of scrapie prion protein: improved purifications and infrared spectra. *Biochemistry.* 50:4479–4490.
6. Baron, G. S., and B. Caughey. 2003. Effect of glycosylphosphatidylinositol anchor-dependent and -independent prion protein association with model raft membranes on conversion to the protease-resistant isoform. *J. Biol. Chem.* 278:14883–14892.
7. Re, F., S. Sesana, …, M. Masserini. 2008. Prion protein structure is affected by pH-dependent interaction with membranes: a study in a model system. *FEBS Lett.* 582:215–220.
8. O'Donovan, C. N., D. Tobin, and T. G. Cotter. 2001. Prion protein fragment PrP-(106–126) induces apoptosis via mitochondrial disruption in human neuronal SH-SY5Y cells. *J. Biol. Chem.* 276:43516–43523.
9. Salmona, M., G. Forloni, …, O. Bugiani. 1997. A neurotoxic and gliotrophic fragment of the prion protein increases plasma. *Neurobiol. Dis.* 57:47–57.
10. Selvaggini, C., L. De Gioia, …, M. Salmona. 1993. Molecular characteristicss of a protease-resistant, amyloidogenic and neurotoxic peptide homologous to residues 106–126 of the prion protein. *Biochem. Biophys. Res. Commun.* 194:1380–1386.

11. Kurganov, B., M. Doh, and N. Arispe. 2004. Aggregation of liposomes induced by the toxic peptides Alzheimer's Abetas, human amylin and prion (106–126): facilitation by membrane-bound GM1 ganglioside. *Peptides.* 25:217–232.
12. Kourie, J. I., P. V. Farrelly, and C. L. Henry. 2001. Channel activity of deamidated isoforms of prion protein fragment 106–126 in planar lipid bilayers. *J. Neurosci. Res.* 66:214–220.
13. Lin, M. C., T. Mirzabekov, and B. L. Kagan. 1997. Channel formation by a neurotoxic prion protein fragment. *J. Biol. Chem.* 272:44–47.
14. Cohen, F. E., and J. W. Kelly. 2003. Therapeutic approaches to protein-misfolding diseases. *Nature.* 426:905–909.
15. Doig, A. J., and P. Derreumaux. 2015. Inhibition of protein aggregation and amyloid formation by small molecules. *Curr. Opin. Struct. Biol.* 30:50–56.
16. Rambold, A. S., M. Miesbauer, …, J. Tatzelt. 2008. Green tea extracts interfere with the stress-protective activity of PrP and the formation of PrP. *J. Neurochem.* 107:218–229.
17. Bieschke, J., J. Russ, …, E. E. Wanker. 2010. EGCG remodels mature alpha-synuclein and amyloid-beta fibrils and reduces cellular toxicity. *Proc. Natl. Acad. Sci. USA.* 107:7710–7715.
18. Ehrnhoefer, D. E., J. Bieschke, …, E. E. Wanker. 2008. EGCG redirects amyloidogenic polypeptides into unstructured, off-pathway oligomers. *Nat. Struct. Mol. Biol.* 15:558–566.
19. Westermark, P. 1972. Quantitative studies on amyloid in the islets of Langerhans. *Ups. J. Med. Sci.* 77:91–94.
20. Höppener, J. W., B. Ahrén, and C. J. Lips. 2000. Islet amyloid and type 2 diabetes mellitus. *N. Engl. J. Med.* 343:411–419.
21. Marzban, L., K. Park, and C. B. Verchere. 2003. Islet amyloid polypeptide and type 2 diabetes. *Exp. Gerontol.* 38:347–351.
22. Sparr, E., M. F. Engel, …, J. A. Killian. 2004. Islet amyloid polypeptide-induced membrane leakage involves uptake of lipids by forming amyloid fibers. *FEBS Lett.* 577:117–120.
23. Jayasinghe, S. A., and R. Langen. 2007. Membrane interaction of islet amyloid polypeptide. *Biochim. Biophys. Acta.* 1768:2002–2009.
24. Weise, K., D. Radovan, …, R. Winter. 2010. Interaction of hIAPP with model raft membranes and pancreatic beta-cells: cytotoxicity of hIAPP oligomers. *ChemBioChem.* 11:1280–1290.
25. Kim, J., H. Cheon, …, M. S. Lee. 2014. Amyloidogenic peptide oligomer accumulation in autophagy-deficient β cells induces diabetes. *J. Clin. Invest.* 124:3311–3324.
26. Zhang, M., B. Ren, …, J. Zheng. 2017. Membrane interactions of hIAPP monomer and oligomer with lipid membranes by molecular dynamics simulations. *ACS Chem. Neurosci.* 8:1789–1800.
27. Engel, M. F., L. Khemtémourian, …, J. W. Höppener. 2008. Membrane damage by human islet amyloid polypeptide through fibril growth at the membrane. *Proc. Natl. Acad. Sci. USA.* 105:6033–6038.
28. Xu, W., G. Wei, …, Y. Mu. 2011. Effects of cholesterol on pore formation in lipid bilayers induced by human islet amyloid polypeptide fragments: a coarse-grained molecular dynamics study. *Phys. Rev. E Stat. Nonlin. Soft Matter Phys.* 84:051922.
29. Sciacca, M. F., J. R. Brender, …, A. Ramamoorthy. 2012. Phosphatidylethanolamine enhances amyloid fiber-dependent membrane fragmentation. *Biochemistry.* 51:7676–7684.
30. Williams, T. L., and L. C. Serpell. 2011. Membrane and surface interactions of Alzheimer's Aβ peptide–insights into the mechanism of cytotoxicity. *FEBS J.* 278:3905–3917.
31. Jelinek, R., and T. Sheynis. 2010. Amyloid - membrane interactions: experimental approaches and techniques. *Curr. Protein Pept. Sci.* 11:372–384.
32. Rai, D. K., V. K. Sharma, …, S. Qian. 2016. Neutron scattering studies of the interplay of amyloid β peptide(1-40) and an anionic lipid 1,2-dimyristoyl-sn-glycero-3-phosphoglycerol. *Sci. Rep.* 6:30983.
33. Sun, Y., W. C. Hung, …, H. W. Huang. 2015. Membrane-mediated amyloid formation of PrP 106–126: a kinetic study. *Biochim. Biophys. Acta.* 1848:2422–2429.
34. Kim, D. H., and J. A. Frangos. 2008. Effects of amyloid β-peptides on the lysis tension of lipid bilayer vesicles containing oxysterols. *Biophys. J.* 95:620–628.
35. George, T. C., D. A. Basiji, …, P. J. Morrissey. 2004. Distinguishing modes of cell death using the ImageStream multispectral imaging flow cytometer. *Cytometry A.* 59:237–245.
36. Phanse, Y., A. E. Ramer-Tait, …, B. H. Bellaire. 2012. Analyzing cellular internalization of nanoparticles and bacteria by multi-spectral imaging flow cytometry. *J. Vis. Exp.* 64:e3884.
37. Barteneva, N. S., E. Fasler-Kan, and I. A. Vorobjev. 2012. Imaging flow cytometry: coping with heterogeneity in biological systems. *J. Histochem. Cytochem.* 60:723–733.
38. Mandal, S. K., R. Biswas, …, A. R. Khuda-Bukhsh. 2010. Lycopodine from Lycopodium clavatum extract inhibits proliferation of HeLa cells through induction of apoptosis via caspase-3 activation. *Eur. J. Pharmacol.* 626:115–122.
39. Domhan, S., L. Ma, …, A. Abdollahi. 2011. Intercellular communication by exchange of cytoplasmic material via tunneling nano-tube like structures in primary human renal epithelial cells. *PLoS One.* 6:e21283.
40. Ahrens, E. T., R. Flores, …, P. A. Morel. 2005. In vivo imaging platform for tracking immunotherapeutic cells. *Nat. Biotechnol.* 23:983–987.
41. Vranic, S., N. Boggetto, …, S. Boland. 2013. Deciphering the mechanisms of cellular uptake of engineered nanoparticles by accurate evaluation of internalization using imaging flow cytometry. *Part. Fibre Toxicol.* 10:2.
42. Moscho, A., O. Orwar, …, R. N. Zare. 1996. Rapid preparation of giant unilamellar vesicles. *Proc. Natl. Acad. Sci. USA.* 93:11443–11447.
43. Dominical, V., L. Samsel, and J. P. McCoy, Jr. 2017. Masks in imaging flow cytometry. *Methods.* 112:9–17.
44. Cao, P., A. Abedini, …, D. P. Raleigh. 2013. Islet amyloid polypeptide toxicity and membrane interactions. *Proc. Natl. Acad. Sci. USA.* 110:19279–19284.
45. Jackson, J. K., and K. Letchford. 2016. The effective solubilization of hydrophobic drugs using epigallocatechin gallate or tannic acid-based formulations. *J. Pharm. Sci.* 105:3143–3152.
46. Zhong, J., W. Zheng, …, Y. Sha. 2007. PrP106–126 amide causes the semi-penetrated poration in the supported lipid bilayers. *Biochim. Biophys. Acta.* 1768:1420–1429.
47. Knight, J. D., J. A. Hebda, and A. D. Miranker. 2006. Conserved and cooperative assembly of membrane-bound α-helical states of islet amyloid polypeptide. *Biochemistry.* 45:9496–9508.
48. Niu, Z., Z. Zhang, …, J. Yang. 2018. Interactions between amyloid β peptide and lipid membranes. *Biochim. Biophys. Acta. Biomembr.* 1860:1663–1669.
49. Walsh, P., G. Vanderlee, …, S. Sharpe. 2014. The mechanism of membrane disruption by cytotoxic amyloid oligomers formed by prion protein (106–126) is dependent on bilayer composition. *J. Biol. Chem.* 289:10419–10430.
50. Pan, J., P. K. Sahoo, …, L. Song. 2017. Membrane disruption mechanism of a prion peptide (106–126) investigated by atomic force microscopy, Raman and electron paramagnetic resonance spectroscopy. *J. Phys. Chem. B.* 121:5058–5071.
51. Brender, J. R., S. Salamekh, and A. Ramamoorthy. 2012. Membrane disruption and early events in the aggregation of the diabetes related peptide IAPP from a molecular perspective. *Acc. Chem. Res.* 45:454–462.
52. Herva, M. E., S. Zibaee, …, M. G. Spillantini. 2014. Anti-amyloid compounds inhibit α-synuclein aggregation induced by protein misfolding cyclic amplification (PMCA). *J. Biol. Chem.* 289:11897–11905.
53. Sheynis, T., A. Friediger, …, R. Jelinek. 2013. Aggregation modulators interfere with membrane interactions of β2-microglobulin fibrils. *Biophys. J.* 105:745–755.